PARAMETRIC DRIVE OF A TOROIDAL MEMS RATE INTEGRATING GYROSCOPE DEMONSTRATING < 20 PPM SCALE FACTOR STABILITY

D. Senkal[1], E.J. Ng[2], V. Hong[2], Y. Yang[2], C.H. Ahn[2], T.W. Kenny[2], and A.M. Shkel[1]
[1]University of California, Irvine, California, USA
[2]Stanford University, Palo Alto, California, USA

ABSTRACT

In this paper, we report parametric drive of a MEMS rate integrating gyroscope for reduction of drifts induced by drive electronics. A Toroidal Ring Gyroscope (TRG) with 100k Q-factor at 1760 µm diameter was fabricated in epitaxial silicon encapsulation (EpiSeal) process. Device was operated in rate integrating mode using a FPGA based control system. In contrast to the conventional amplitude control architecture, the central star electrode of the gyroscope, connected to a single drive channel was utilized for amplitude control of both modes. Due to the parametric pumping effect, energy added to each (x and y) mode is proportional to the existing amplitude of the respective mode. As a result, errors associated with finding the orientation of the standing wave and x-y drive gain drift are bypassed. Compared to conventional x-y drive architecture, as high as 14x improvement in scale factor stability was observed with parametric pumping, resulting in better than 20 ppm scale factor stability without any compensation or temperature stabilization.

INTRODUCTION

Degenerate mode Coriolis Vibratory Gyroscopes (CVGs) can be instrumented in two primary modes of operation: (1) rate gyroscope mechanization where the standing wave pattern is locked to a fixed orientation, (2) rate integrating (whole angle) gyroscope mechanization, where the standing wave is free to rotate under the effect of Coriolis forces. Rate integrating gyroscope offers a number of unique advantages compared to conventional vibratory rate gyroscopes, including mechanically unlimited dynamic range, low noise due to degenerate mode operation, and exceptional scale factor stability.

All axi-symmetric MEMS gyroscope architectures are capable of whole angle mechanization. Examples include ring gyros [1], disk gyros [2, 3], and 3-D wineglass gyroscopes [4, 5]. Typically, these architectures utilize two sets of drive electrodes for the two resonant modes of the gyroscope. As a result, amplitude control in whole angle mechanization would require finding the orientation of the standing wave and pumping energy along this direction using two sets of drive electrodes (vector drive). However, this method is susceptible to drift due to gain unbalance in drive electronics, errors in calculating the angle of the standing wave, as well as, the time delay between estimation of the standing wave and the actual amplitude command.

In this work, we explore parametric drive for amplitude control of MEMS rate integrating gyroscopes, which has previously been reserved for high performance macro-scale Vibratory Gyros [6]. In contrast to conventional amplitude control, a single drive channel connected to the central star electrode of the gyroscope was utilized for amplitude control of both modes (scalar drive). Even though a single drive channel is used, due to the parametric pumping effect, energy added to each (x and y) mode is proportional to the existing amplitude of the respective mode. This permits amplitude control of the standing wave at any arbitrary angle with minimal amount of perturbation. The scalar nature of the amplitude controller helps bypass errors associated with finding the orientation of the standing wave, time delay in the calculation, and x-y drive gain drift.

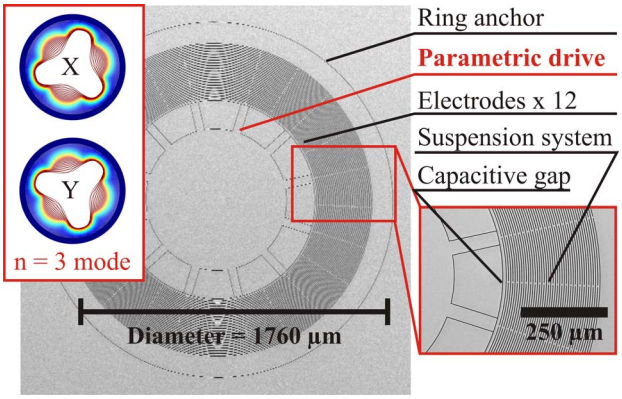

Figure 1: A 100k Q-factor, epitaxial silicon encapsulated Toroidal Ring Gyroscope was used in the experiments [7]. Device consists of an outer ring anchor, distributed suspension system and an inner electrode assembly.

An additional benefit of parametric drive of MEMS gyroscopes is the minimization of the electrical feed-through between the actuation and pick-off channels [8, 9]. For a conventional MEMS gyroscope, actuation and pick-off signals occur at the same frequency. Any feed-through from the actuation signal will corrupt the pick-off channel, lowering overall performance of the system. Parametric drive mitigates this problem by separating the frequency of drive and pick-off channels. Since parametric drive frequency is a multiple of systems drive frequency, the electrostatic feed-through into the sense channel can be filtered out.

DESIGN

Gyroscope Architecture

A Toroidal Ring Gyroscope (TRG) with Q-factor of 100k at 70 kHz central frequency and 1.7 mm diameter was used for the experiments; the device consists of an outer ring anchor surrounding a distributed mass system and central electrode architecture [7], Fig. 1. As opposed to other axi-symmetric devices with central support structures vibration energy of TRG is concentrated at the innermost ring, Fig. 2. The distributed support structure decouples the vibrational motion from the substrate. This decoupling mitigates anchor losses into the substrate and prevents die/package stresses from propagating into the vibratory structure.

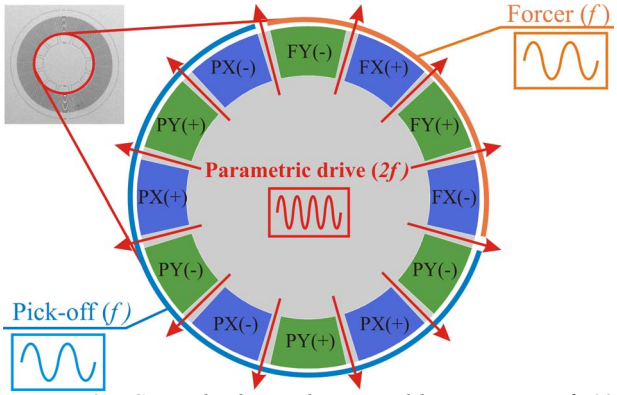

Figure 2: Central electrode assembly consists of 12 discrete electrodes, divided into 4 drive and 8 pick-off electrodes, and one star shaped parametric electrode.

Fabrication

The Toroidal Ring Gyroscope (TRG) was fabricated using a wafer-level epitaxial silicon encapsulation process (EpiSeal) [10]. EpiSeal process utilizes epitaxially grown silicon to seal the device layer at extremely high temperatures, which results in an ultra-clean wafer-level seal. This results in high vacuum levels (as low as 1 Pa) without the need for getter materials for absorption of sealing by-products. The epi-seal encapsulation process was proposed by researchers at the Robert Bosch Research and Technology Center in Palo Alto and then demonstrated in a close collaboration with Stanford University. This collaboration is continuing to develop improvements and extensions to this process for many applications, while the baseline process has been brought into commercial production by SiTime Inc.

Electrode Architecture

Device is operated in n = 3 mode, to help reduce the frequency splits associated with n = 2 mode on <100> silicon. Electrode assembly is located at the center of the gyroscope and consists of twelve discrete electrodes and one central star electrode, Fig 2. Discrete electrodes are distributed in groups of six onto the two degenerate wineglass modes. Out of six electrodes, two electrodes were used as a forcer and four as a pick-off for each mode, giving a total of four forcer and eight pick-off electrodes across the gyro.

In this work, the central star-shaped electrode is used for parametric pumping. Due to the twelve-pointed circular nature of this electrode, parametric pumping has equal contribution to the both degenerate n = 3 wineglass modes.

Control System

A Kintex 7 FPGA was used for controlling the gyro. The key component of this approach is a PLL loop that tracks the gyro motion at any arbitrary pattern angle as opposed to locking onto one of the primary gyro axis. Once the PLL lock is established, the FPGA extracts the slow moving variables: amplitude (E), quadrature error (Q), and pattern angle (θ) using the equations presented in

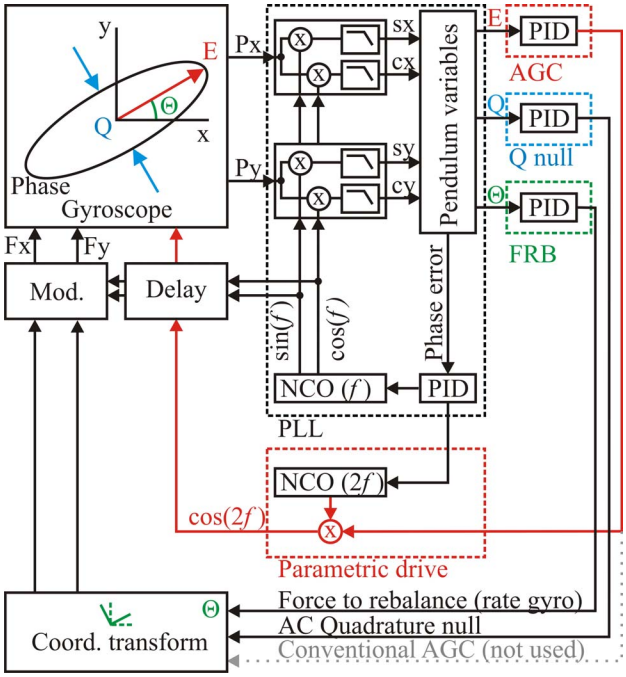

Figure 3: Rate integrating gyro controller with parametric drive, implemented on a Kintex 7 FPGA running at 1 MHz.

[11], Fig 3. A PID controller acts on each of these variables. These are Amplitude Gain Control (AGC) acting on E, quadrature null acting on Q and force-to-rebalance (FRB) that controls pattern angle (θ). For the whole angle mechanization, FRB is disabled so that the standing wave is free to precess. Once the correct command voltages for E, Q and θ are established, a coordinate transform around θ is performed to align these signals to the standing wave. This is followed by modulation of the command voltages at PLL frequency.

For the, parametric drive, a secondary numerically controlled oscillator (NCO) is used to generate a sine wave at twice the PLL frequency. This signal is applied to the central star-shaped electrode to parametrically pump energy in x-y plane at twice the resonance frequency, Fig 2. Due to the parametric pumping effect, energy added to each (x and y) mode is proportional to the existing amplitude of the respective mode [8]:

$$\ddot{x} + \frac{\omega_x}{Q_x}\dot{x} + \left(\omega_x^2 + \frac{F_p}{m_{eq}}\sin(2\omega t + \phi_p)\right)x = \frac{F_x}{m_{eq}}\sin(\omega t + \phi_f) + 2\eta\,\dot{y}\Omega_z, \quad (1)$$

$$\ddot{y} + \frac{\omega_y}{Q_y}\dot{y} + \left(\omega_y^2 + \frac{F_p}{m_{eq}}\sin(2\omega t + \phi_p)\right)y = \frac{F_y}{m_{eq}}\sin(\omega t + \phi_f) - 2\eta\,\dot{x}\Omega_z, \quad (2)$$

where ω_x, ω_y and Q_x, Q_y are the resonance frequencies and the Q-factors of the two degenerate modes, m_{eq} is the equivalent mass of the vibratory system, η is the angular gain factor, ω is the drive frequency and ϕ_p, ϕ_f are the phase of the parametric and vector drives respectively.

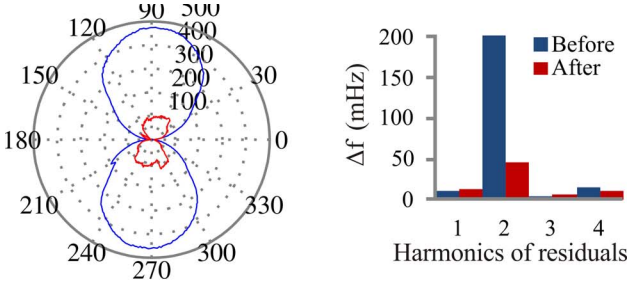

a) PLL frequency (Δf) with respect to pattern angle (mHz).

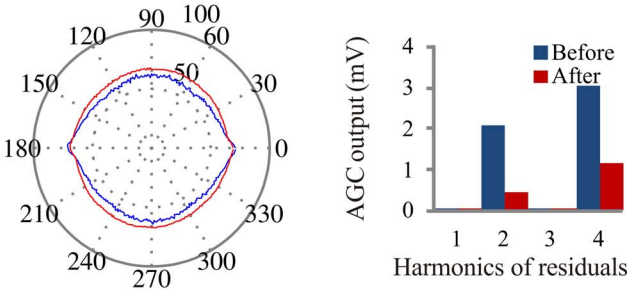

b) Parametric drive amplitude gain control (AGC) output (mV).

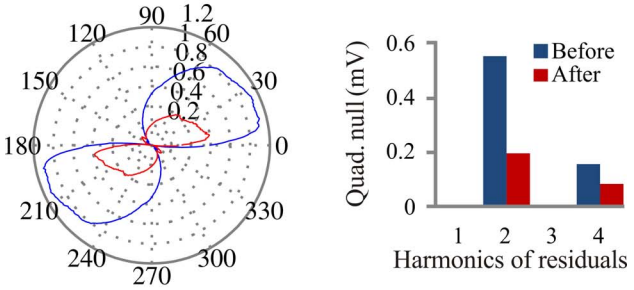

c) Quadrature null control output (mV).

Figure 4: Tuning of the gyro based on residuals of pattern angle data from PLL, parametric AGC and quadrature null loops.

This creates a preferential direction of pumping along the orientation of the standing wave without the need for any coordinate transformation around θ:

$$\theta = atan(\frac{y}{x}) \quad (3)$$

Open loop parametric drive is typically unstable for nominal drive amplitudes [8, 9], which causes the gyro amplitude to increase exponentially for a fixed parametric drive signal. For this reason a secondary AGC controls the parametric drive voltage as to keep the gyro amplitude stable. This closed loop operation permits parametric drive of the gyro at a wide range of drive amplitudes, outside the stability boundary of open loop parametric drive.

Typical gyro startup procedure begins with driving the gyro to a preset amplitude using conventional (at resonance) drive. Once the PLL and AGC stabilize, drive signal is disabled and immediately parametric drive AGC is enabled. This switch occurs within one clock cycle of the FPGA and eliminates over-shoots in drive amplitude, which would otherwise occur while starting up the high-Q resonator.

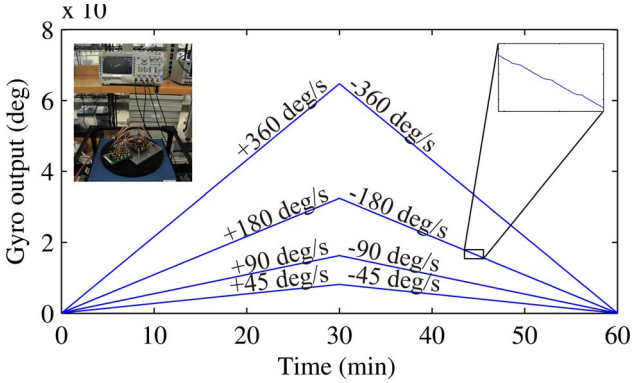

Figure 5: Experimental demonstration of rate integrating operation under parametric drive.

EXPERIMENTAL RESULTS

Pattern Angle Data

Pattern angle data for the gyroscope was obtained by changing the orientation of the standing wave (θ) using the force-to-rebalance loop and recording the gyro output with respect to pattern angle (θ). Fourier series expansion of pattern angle data from PLL, quadrature, and AGC loops was used for calibrating the gyro. Second harmonic of the PLL output provides run-time identification of the frequency split (Δf), which was used to tune the frequency split down to 50 mHz (700 ppb). Parametric AGC command signal displayed a 2 mV (~4%) variation on second harmonic, which was attributed to pick-off gain unbalance between x and y modes. Adjusting the pick-off gains in the FPGA, reduced this unbalance down to < 0.5 mV. The combined effect of tuning the frequency split and the pick-off gain unbalance resulted in an overall 2.5x reduction in the required quadrature null command signal, Fig 4.

Rate Integrating Gyro Response

In order to test the rate integrating operation, the gyro was driven using parametric drive and a constant rotation rate was applied for 1 hour, switching the direction at 30 minutes mark. Fig. 5 shows the unwrapped gyro response for four different speeds. This experiment was later repeated using conventional (vector) drive. A linear fit to the data revealed a combined electrical/mechanical angular gain factor of ~0.6. Comparison of residuals from both experiments is shown in, Fig 6. For all rate inputs the parametric drive resulted in better scale factor stability compared to conventional drive architecture. As predicted, the highest difference between conventional drive and parametric drive occurred at higher rotation rates. Time lag in calculation of the drive vector becomes more important at higher rotation rates as this lag can cause the drive vector to couple into the gyro output. As a result, any change in the drive vector amplitude either due to drive gain drifts or a Q-factor change in the resonator element can affect scale factor stability.

For 360°/s rate input over a 30 minute period standard deviation of accumulated error for conventional drive was 176° versus 13° for parametric drive. This resulted in 14x improvement for parametric drive and < 20 ppm scale factor stability overall, without any compensation or temperature stabilization.

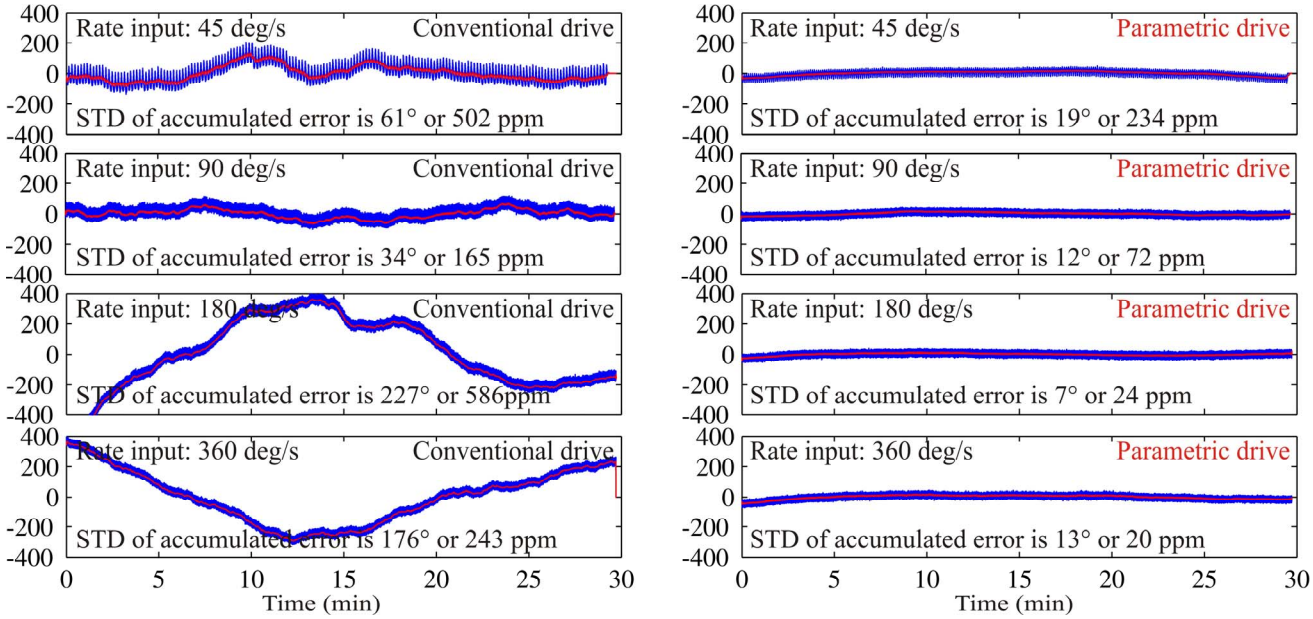

Figure 6: Comparison of residual errors of conventional drive and parametric drive for different rate inputs.

CONCLUSIONS

Parametric drive of a MEMS rate integrating gyroscope was presented for the first time. Parametric pumping was used to bypass the errors associated with finding the orientation of the standing wave, time delay in the calculation and x-y drive gain drift. This resulted in as high as 14x improvement in scale factor stability compared to conventional x-y drive and better than 20 ppm scale factor stability without any compensation or temperature stabilization. In addition, parametric drive reduces drive to pick-off electrical feed-through by creating a frequency separation between drive and pick-off channels.

Techniques presented in this paper can be used to improve performance of other axi-symmetric gyro architectures, such as ring, disk, and wineglass gyros.

ACKNOWLEDGEMENTS

Design and characterization of devices was done in UCI Microsystems Laboratory, fabrication was done at Stanford Nanofabrication Facility. This work was supported in part by the Defense Advanced Research Projects Agency Precision Navigation and Timing Program managed by Dr. A. Shkel and Dr. R. Lutwak under Contract N66001-12-1-4260, and in part by the National Science Foundation through the National Nanotechnology Infrastructure Network under Grant ECS-9731293

REFERENCES

[1] F. Ayazi and K. Najafi, "Design and fabrication of high-performance polysilicon vibrating ring gyroscope," in *IEEE MEMS*, Heidelberg, Germany, 1998, pp. 621-626.

[2] Z. Hao, S. Pourkamali, and F. Ayazi, "VHF single-crystal silicon elliptic bulk-mode capacitive disk resonators-part I: design and modeling," in *IEEE/ASME JMEMS*, 13, (6), pp. 1043–1053, 2004.

[3] T. H. Su, S. H. Nitzan, P. Taheri-Tehrani, M. H. Kline, B. E. Boser, and D. A. Horsley, "Silicon MEMS Disk Resonator Gyroscope with an Integrated CMOS Analog Front-End," in *IEEE Sensors Journal*, 14, (10), pp. 3426–3432, 2013.

[4] D. Senkal, M. J. Ahamed, S. Askari, and A. M. Shkel, "1 million Q-factor demonstrated on micro-glassblown fused silica wineglass resonators with out-of-plane electrostatic transduction," in *Hilton Head*, Hilton Head Island, SC, USA, 2014, pp. 68–71.

[5] J. Cho, J.-K. Woo, J. Yan, R. L. Peterson, and K. Najafi, "A high-Q birdbath resonator gyroscope (BRG)," in *TRANSDUCERS*, Barcelona, Spain, 2013, pp. 1847–1850.

[6] D. M. Rozelle, "The hemispherical resonator gyro: From wineglass to the planets," in *AAS/AIAA Space Flight Mechanics Meeting*, 2009, pp. 1157–1178.

[7] D. Senkal, S. Askari, M. J. Ahamed, E. J. Ng, V. Hong, Y. Yang, C. H. Ahn, T. W. Kenny, and A. M. Shkel, "100k Q-factor toroidal ring gyroscope implemented in wafer-level epitaxial silicon encapsulation process," in *IEEE MEMS,* San Francisco, California, USA, 2014, pp. 9–12.

[8] K. M. Harish, B. J. Gallacher, J. S. Burdess, and J. A. Neasham, "Experimental investigation of parametric and externally forced motion in resonant MEMS sensors," in *IOP JMM*, 19, (1), pp. 15-21, Jan. 2009.

[9] L. A. Oropeza-Ramos, C. B. Burgner, and K. L. Turner, "Robust micro-rate sensor actuated by parametric resonance," *Sensors and Actuators A: Phyical.*, 152, (1), pp. 80–87, 2009.

[10] R. N. Candler, M. A. Hopcroft, B. Kim, W-T. Park, R. Melamud, M. Agarwal, G. Yama, A. Partridge, M. Lutz, T. W. Kenny, "Long-Term and Accelerated Life Testing of a Novel Single-Wafer Vacuum Encapsulation for MEMS Resonators," in *IEEE/ASME JMEMS*, 15, (6), pp. 1446-1456, 2006.

[11] D. D. Lynch, "Vibratory gyro analysis by the method of averaging," in *Intl. Conf. on Gyroscopic Tech. and Navigation,* St. Petersburg, Russia, 1995, pp. 26-34.

CONTACT

*D. Senkal, tel: +1-949-945-0858; dsenkal@uci.edu.